We are IntechOpen, the world's leading publisher of Open Access books
Built by scientists, for scientists

4,800
Open access books available

122,000
International authors and editors

135M
Downloads

Our authors are among the

154
Countries delivered to

TOP 1%
most cited scientists

12.2%
Contributors from top 500 universities

CLARIVATE ANALYTICS
BOOK CITATION INDEX
INDEXED

WEB OF SCIENCE™

Selection of our books indexed in the Book Citation Index in Web of Science™ Core Collection (BKCI)

Interested in publishing with us?
Contact book.department@intechopen.com

Numbers displayed above are based on latest data collected.
For more information visit www.intechopen.com

Chapter 4

Removal of Phenol from Wastewater Using Fenton-Like Reaction over Iron Oxide–Modified Silicates

Agnieszka Węgrzyn

Additional information is available at the end of the chapter

http://dx.doi.org/10.5772/65097

Abstract

Iron-containing active phase was deposited on natural layered silicate (vermiculite) using several techniques such as ion exchange, precipitation, and forced hydrolysis during hydrothermal digestion. Tuning of the synthesis conditions resulted in preparation of the catalysts with different loading of active phase and physicochemical properties. The composite materials were characterized with respect to their structure (X-ray diffraction), agglomeration state of Fe (diffuse reflectance UV-vis spectroscopy), and chemical composition. Catalytic tests were performed in semi-batch reactor under atmospheric pressure. Aqueous solution of phenol was used as a model industrial effluent, and hydrogen peroxide was added as an oxidant. Spectral techniques were used for identification of intermediate oxidation products. Spent catalysts were also characterized, and structural and chemical changes were determined, e.g., leaching degree of active phase.

Keywords: Fenton-like process, advanced oxidation processes, catalysis, silicate, vermiculite, nanocrystalline iron oxide, phenol

1. Introduction

Refractory organic compounds, such as dyes, phenols, or endocrine disrupting compounds (EDC), are characterized with high toxicity, carcinogenic properties, and this poses a serious hazard to aquatic living organisms. Difficulty of contaminations' removal is caused by their resistance to aerobic digestion, stability to light, heat, and oxidizing agents. Technologies used currently for wastewater treatment, however, used widely, suffer from design shortcomings or are very expensive. Emerging technologies, so-called advanced oxidation processes (AOP), is

INTECH
open science | open minds

© 2017 The Author(s). Licensee InTech. This chapter is distributed under the terms of the Creative Commons Attribution License (http://creativecommons.org/licenses/by/3.0), which permits unrestricted use, distribution, and reproduction in any medium, provided the original work is properly cited. CC BY

a large group of methods based on oxidation using strong oxidants, such as ozone or hydrogen peroxide. In AOP methods, higher conversion levels may be obtained at atmospheric pressure and temperatures lower compared to other oxidation processes [1–6]. Moreover, chemical oxidants may be accompanied by catalysts or physical agents such as sunlight, UV or γ radiation, ultrasounds, microwave, or cavitation, increasing efficiency of the reaction [7, 8].

The catalysts used in the Fenton-like system are, among others, natural iron-bearing earth materials, such as goethite, hematite, magnetite, or ferrihydrite [9–11]. Modification of iron oxides to improve their performance in organic pollutant degradation can be achieved by substitution with other transition metals [12]; however, introduction of heavy metals may be questionable from the point of view of the secondary contamination with catalytic leachates. It is also known that nanoscale materials are characterized with different properties compared to their bulk phase [8, 13, 14]. Nanocatalysts offer higher specific surface areas and few or no mass-transfer limitations. It is expected that reaction rate will be higher for nanomaterials. Also, diffusion of large organic molecules (organic dyes, pharmaceuticals) will be no longer problematic as it is observed in microporous materials. On the other hand, the separation and recycling of nanocatalysts at a technical scale still present a challenge.

To circumvent the costly catalyst separation process, magnetic properties of some iron oxides may be exploited [15, 16]. The other possibility is the immobilization on solid support. The most popular materials in this group are activated carbon, silica, and aluminum oxide [17–21]; however, more advanced technologies are also studied employing graphene oxide [22]. The encapsulation of iron oxide nanoparticles in polymer matrix or carbonized sewer sludge was reported as another possibility to stabilize oxide nanoparticles [23, 24].

Facing much more stringent environmental regulations, new waste-free technologies must be developed, based on cheaper, non-toxic materials. Clays proposed as starting materials fulfill all requirements for low-cost, ecological precursors for industrial technologies or large-scale applications. Such materials could be used as catalysts in a large group of emerging technologies consisting on oxidation processes, such as wet oxidation, catalytic wet air oxidation, and advanced oxidation processes. Natural clay minerals provide with excellent support for Fe-containing nanocrystalline active phase of the Fenton-like reaction. Vermiculite, which was used in presented work as a catalytic support, is natural clay mineral belonging to phyllosilicates. It is characterized with high thermal and mechanical stability. Moreover, its properties may be easily modified to obtain efficient adsorbents or catalysts [25, 26].

2. Materials and methods

Commercial expanded vermiculite (South Africa), fraction size 0.5–2 mm, was provided by Romico Polska Sp. z o.o. The silicate was pulverized in electrical blender, and fraction below 180 μm was separated (sample S0). Such prepared vermiculite was used as a support for deposition of nanocrystalline iron oxides.

Two standard procedures [27, 28] were applied to obtain well-defined oxide structures. Pure 2-line ferrihydrite was prepared by precipitation from 0.1 M $Fe(NO_3)_3 \cdot 9H_2O$ (p.a., POCh)

http://dx.doi.org/10.5772/65097

solution using 1 M KOH (p.a., POCh). Potassium hydroxide solution was added dropwise at RT and constant stirring until pH was equal to 7. Product was centrifuged, washed with water, and freeze dried. Similar procedure was used to obtain vermiculite-supported ferrihydrite. Suspension of 5 g of vermiculite (S0) was prepared in 150 mL of distilled water, then 100 mL of $Fe(NO_3)_3 \cdot 9H_2O$ solution was added dropwise. Suspension was stirred for the next 2 h to allow ion exchange. In the next step, 1 M KOH solution was added to raise pH up to 7. Crystallization was continued for the next 30 min, product was centrifuged, washed, and dried. Sample codes, depending on Fe/vermiculite ratio, were S2, S3, and S4 (**Table 1**).

Sample name (precipitation)	Sample name (forced hydrolysis)	Fe/vermiculite ratio (mg/g)
S0	HS0	–
–	HS1	16.8
S2	HS2	33.6
S3	HS3	67.2
S4	–	134.4

Table 1. Intended Fe/vermiculite ratio in vermiculite-supported Fe oxide catalysts.

Pure hematite with crystal size of 4 nm was prepared by forced hydrolysis. 3.32 g of Fe(NO3)3·9H2O was dissolved in preheated HCl (p.a., POCh) solution (0.002 M, 400 mL) to obtain Fe concentration of 0.02 M.. Solution was transferred into polypropylene bottle fitted in autoclave and heated at 98°C for 7 days. Product was centrifuged, washed with water, and freeze dried. Synthesis of vermiculite-supported nano-hematite was performed using acidified iron nitrate solutions with the addition of 20 g of vermiculite. Sample codes, depending on Fe/vermiculite ratio, were HS0 (no Fe salt was added), HS1, HS2, and HS3 (**Table 1**).

Phenol removal was studied as a test reaction, and semi-batch reactor was used to minimize formation of side products [26]. Round-bottom flask equipped with reflux condenser was heated to 70°C on magnetic stirrer. Each time reactor was charged with 340 mL of phenol solution (pH = 5.4) and 600 mg of catalyst. Hydrogen peroxide (30%, p.a., POCh) was added into the reaction mixture in 13-min intervals (10 min of non-disturbed reaction and 3 min for sample withdrawal and next injection). Phenol concentration was studied spectrophotometrically (Thermo SCIENTIFIC EVOLUTION 220) as a complex with 4-aminoantipyrine. H_2O_2 concentration (using VO_3^- in 8 M H_2SO_4), Fe dissolved in reaction mixture (SCN^- complex), and colored intermediate products (sample quenched with methanol) were also determined spectrophotometrically. In each interval, pH was measured. Reaction conditions were summarized in **Table 2**.

Reaction code	Phenol concentration (g/L)	H_2O_2 volume added in one injection (mL)
Catalyst R1	1	2
Catalyst R01	0.1	2
Catalyst R01m	0.1	0.2

Table 2. Reaction conditions of phenol removal over vermiculite-supported iron oxide catalysts.

The conversion, X (%), of model pollutant (phenol) was calculated according to Eq. (1):

$$X = \frac{C_0 - C}{C_0} \cdot 100\% \tag{1}$$

where C_0 is the starting concentration and C is the concentration at a given reaction time.

Fresh and spent catalysts were characterized by X-ray diffraction method (XRD) using a powder diffractometer (Bruker, D2 PHASER) equipped with CuKα radiation source. The Sherrer equation (2) was used for determination of nano-hematite crystal size:

$$D = \frac{0.89\lambda}{\beta cos\theta} \tag{2}$$

where λ is the X-ray wavelength, β is the line broadening at half the maximum intensity, and θ is the Bragg angle.

The coordination and aggregation of iron present in the catalysts were studied by diffuse reflectance-UV-vis spectroscopy (DRS-UV-vis). The measurements were performed in the range of 190–900 nm with a resolution of 2 nm using an Evolution 600 (Thermo) spectrophotometer. Content of iron was measured using spectrophotometric technique at wavelength λ = 510 nm (Thermo SCIENTIFIC EVOLUTION 220) as a complex with 1,10-phenanthroline after leaching of metal cations in 6 M HCl.

3. Results and discussion

3.1. Catalytic tests

Three types of catalytic tests were carried out in semi-batch reactor: concentrated (R1—1 g/L) and diluted (R01—0.1 g/L) phenol solutions with the addition of significant excess of oxidant (six times 2 mL) and diluted phenol solution with the minimum amount of oxidant added (six times 0.2 mL). In each series of catalytic tests, it was observed that initiation phase is the first step, as in the case of free-radical reactions, especially for experiments carried out in concentrated phenol solution (**Figure 1A**). Initial 10–20 min are characterized with slow increase in pollutant conversion. After 30–50 min of the reaction over iron oxide-containing catalysts, conversion rapidly increased reaching values above 95%. Non-modified silicates, on the other hand, presented very low activity. Sample submitted to hydrothermal treatment (HS0) slightly increased phenol oxidation compared to non-catalytic process; however, in the latter case, conversion was not higher than 8% after 75 min. On the contrary, the addition of starting vermiculite (S0) to reaction mixture resulted in slow increase in phenol conversion up to 42%. Reduction in particle size was the only preparation step in this case; therefore, contaminations present in the starting materials, such as interlayer and adsorbed transition metal cations as

http://dx.doi.org/10.5772/65097

well as naturally occurring iron oxides and carbonates, may be responsible for the observed catalytic effect.

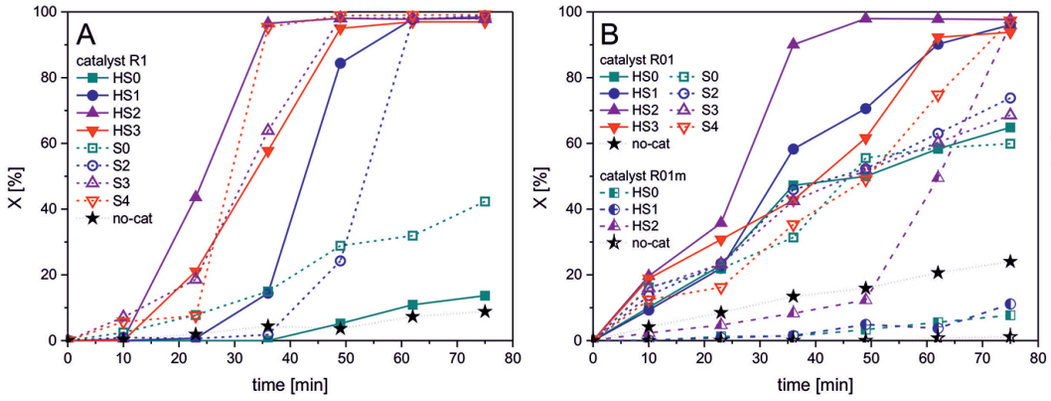

Figure 1. Conversion of phenol in oxidation reaction over vermiculite-supported iron oxide catalysts; A—initial concentration of phenol 1 g/L, volume of H_2O_2 injection = 2 mL; B—initial concentration of phenol 0.1 g/L, volume of H_2O_2 injection = 2 or 0.2 mL.

When diluted solution of phenol was used (**Figure 1B**) and accompanied by small excess of oxidant (R01m—0.2 mL), almost no effect was observed within assigned experimental time. Only one sample, doped with nano-hematite, HS2, showed catalytical properties after 50 min of reaction. The non-catalytical reaction performed with large excess of oxidant (R01—2 mL) resulted in quite significant conversion equal to 48% within 75 min. Slightly higher activity was observed when ferrihydrite-doped samples, S2 and S3, and non-modified silicates were added as catalysts. After constant gradual increase of conversion, it reached 60–75% within 75 minutes. Only one sample with the highest loading of ferrihydrite and samples doped with nano-hematite allowed to reach the conversion level above 95%. Nevertheless, it should be stressed that after initial increase in conversion, it was inhibited and much slower at longer reaction times in the case of removal of concentrated pollutant. Similar effect of the reaction stagnation, due to accumulation of the reaction products, was also observed in homogeneous Fenton reaction [29].

It may be observed that conversion of phenol was more effective with higher doping with ferrihydrite. On the contrary, regardless reaction conditions, in the series of nano-hematite-containing catalysts, an optimum amount of iron oxide results in higher efficiency of the reaction. The best sample in this case was HS2 doped with 3.36 wt.% of iron in the form of nano-hematite.

According to results of the catalytic tests described above, 2-line ferrihydrite supported on vermiculite is less active than analogous materials containing hematite. Additional experiment, performed in concentrated phenol solution (1 g/L) and using active sample HS3 as catalyst, provided information about reaction path and intermediate products. UV-vis spectra for samples withdrawn during experiment, quenched with methanol or mixed additionally with VO_3^-/H_2SO_4 solution, allowed to distinguish between transition products formed in the course of the reaction. After 29 min of the reaction, which corresponds to 43% of phenol

conversion, colored products were formed. In the UV-vis spectrum recorded in methanol (**Figure 2A**) bands assigned to phenol (278 and 284 nm), hydroquinone (300 nm) and benzoquinone/quinhydrone (245, 255, and 300 nm) were identified. However, bands assigned to catechin were strongly overlapped by other strong peaks, and it cannot be excluded that this product was also formed. After 62 min of the experiment phenol conversion reached 97%, no colored products were recorded, and reaction was completed.

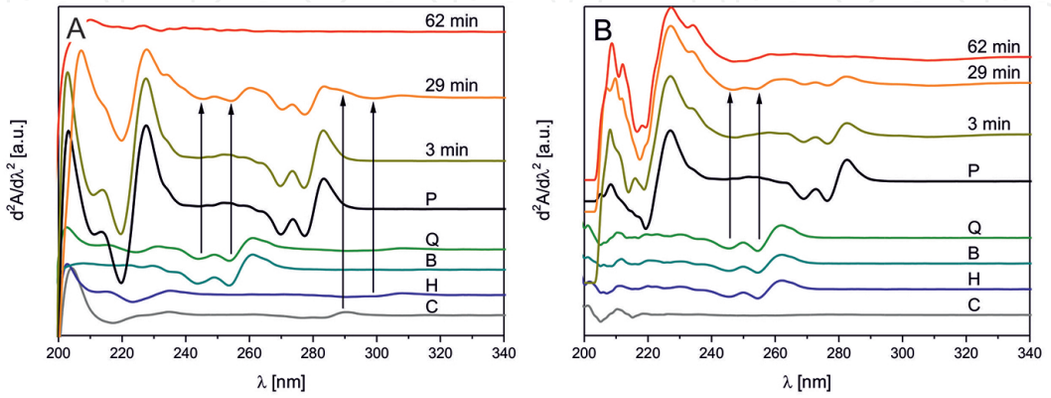

Figure 2. Identification of transition products of phenol oxidation over HS3 catalyst (reaction conditions: PhOH = 1 g/L, volume of H_2O_2 injection = 2 mL): A—derivative UV-vis spectra recorded in MeOH, B—derivative UV-vis spectra recorded in VO_3^-/H_2SO_4; P—phenol; Q—qiunhydrone; B—benzoquinone; H—hydroquinone; C—catechin.

However, in the spectra measured after the reaction of the sample of effluent with VO_3^-/H_2SO_4 mixture (**Figure 2B**), peaks below 230 nm, assigned to unidentified organic compounds, were recorded at the end of the test. Evolution of pH followed opposite trend as phenol conversion, and at 29 and 62 min, it was equal to 2.87 and 2.48, respectively. Those observations confirm that final products are not only H_2O and CO_2 but also organic acids.

3.2. Characterization of as received and spent catalysts

Iron oxide-bearing catalysts were obtained by direct deposition of formed oxide on the silicate support. Vermiculite was selected due to its mechanical and thermal stability. On the contrary to montmorillonite, it is not exfoliating rapidly in contact with water, and swelling is limited to changes of number of water molecules in the interlayer space. Moreover, mineral itself contains significant amount of iron.

As it was shown in **Figure 3**, both expected oxide structures were formed [27, 28]. XRD pattern of 2-line ferrihydrite consists of two broad reflections, while nano-hematite is characterized by the presence of several sharp but not intense peaks. Ferrihydrite structure was not observed after deposition on the support due to inherent poor ordering of the structure and low content in the composite material. On the other hand, using the Sherrer equation, it was confirmed that crystal size of pure nano-hematite phase was 4 nm. Only traces of nano-hematite could be identified in two vermiculite-supported samples with the highest loading of deposited phase —HS2 (3.36 Fe wt.%) and HS3 (6.72 Fe wt.%). Therefore, it was not possible to determine precise crystal parameters for oxide phase.

http://dx.doi.org/10.5772/65097

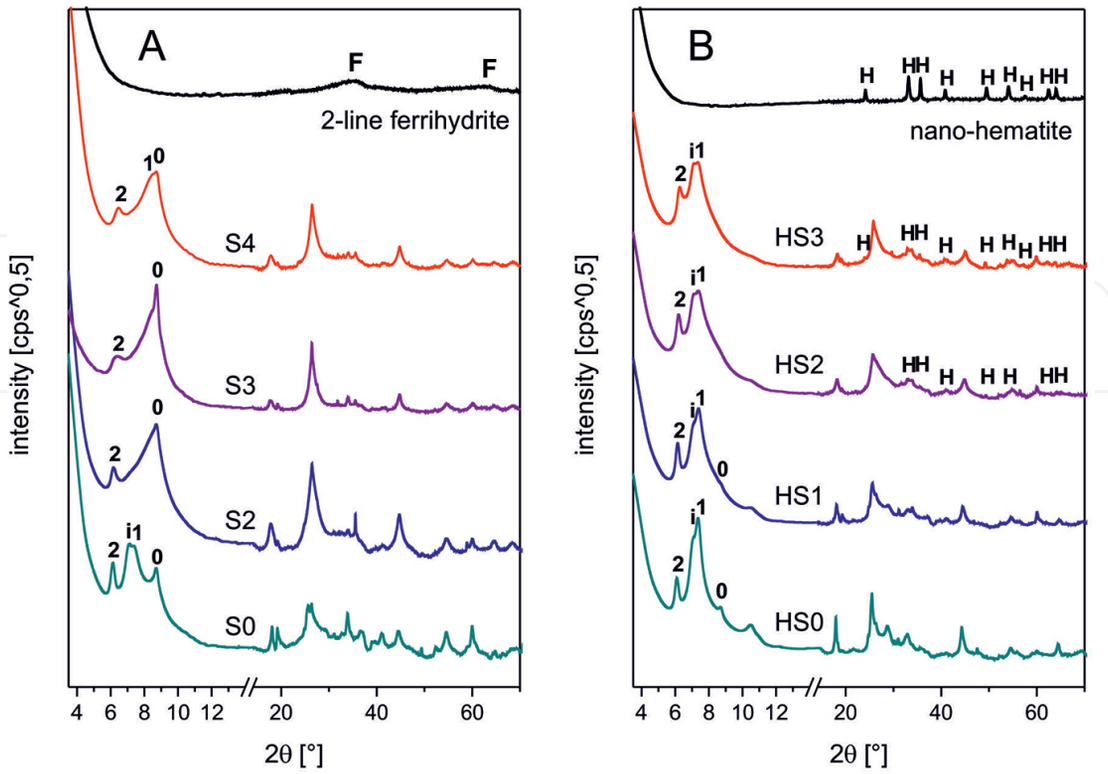

Figure 3. Structure of vermiculite-supported ferrihydrite- (A) and nano-hematite-containing (B) catalysts; F—ferrihydrite; H—nano-hematite; 0, 1, 2—basal reflections of vermiculite corresponding to 0, 1, and 2 layers of interlayer water; i—interstratified vermiculite phases.

Changes in vermiculite structure reflected chemical modifications performed in each synthesis. Starting material (S0) was characterized with complex pattern typical for vermiculites both containing in the interlayer divalent cations and collapsed structure (0 layers of water). Moreover, the interlayer cations are accompanied with 1 or 2 layers of water. Additional peaks below 8° 2θ were assigned to interstratified contracting and non-contracting phases [30].

Upon hydrothermal treatment in the sample HS0 intensity of peak corresponding to one water layer increased, while disappeared peak assigned to the collapsed structure. In the synthesis of 2-line ferrihydrite composite (**Figure 3A**), a first step consisted on an ion exchange of interlayer anions for iron. As a result, peak at 1.40–1.43 nm may be observed; however, it was shifted to lower values for higher loadings of iron oxide: 1.39 and 1.37 nm for S3 and S4, respectively. Described phenomenon is a result of partial dehydration of the interlayer gallery and formation of so-called HIV—hydroxy-interlayered vermiculites [31, 32]. Similar shift was observed also for the sample with the highest nano-hematite content: HS3—1.39 nm.

Application of potassium hydroxide, however, resulted in a deeper rearrangement of interlayer space. Both peaks assigned to interstratification and one water layer almost disappeared. On the other hand, intercalation of K^+ resulted in a large increase in peak intensity at 1 nm [33]. On the contrary, in the samples doped with nano-hematite in hydrothermal conditions (**Figure 3B**), peak assigned to 0 layers of interlayer water decreased with increasing amount of oxide.

In the structure of spent catalysts, traces of hematite were still possible to identify; however, other changes concerning catalyst properties were noticed. Vermiculite support upon reaction in concentrated solution was transformed into Mg^{2+}/Fe^{3+} intercalated structure containing 2 layers in water molecules (**Figure 4A**). In the samples doped with ferrihydrite, only traces of interlayer potassium were preserved, and interlayer spaces were occupied with di- and trivalent cations released from silicate matrix. Hydration state and the number of water molecules strongly depended on the initial amount of iron oxide—the lower doping level the easier rehydration proceeded. Similar dependence was observed also for nano-hematite deposited samples. Such phenomenon should be explained as a result of blocking of interlayer spaces with iron hydroxides. Moreover, iron oxide particles, which were grown near the edges of vermiculite layers, may act as cementing agent, preventing structure swelling. It was also observed that rehydration of the structure depends on the reaction conditions (**Figure 4B**): the higher concentration of phenol and hydrogen peroxide, the easier intercalation of water molecules. As it was shown in **Figure 4C/D**, swelling intensity, which may be expressed as peaks 1.42 (2 layers of water) and 1.20 nm (1 layer of water) intensity ratio, increased at higher concentration of substrates. It cannot be excluded that acidic reaction products also enhanced structural changes of vermiculite support.

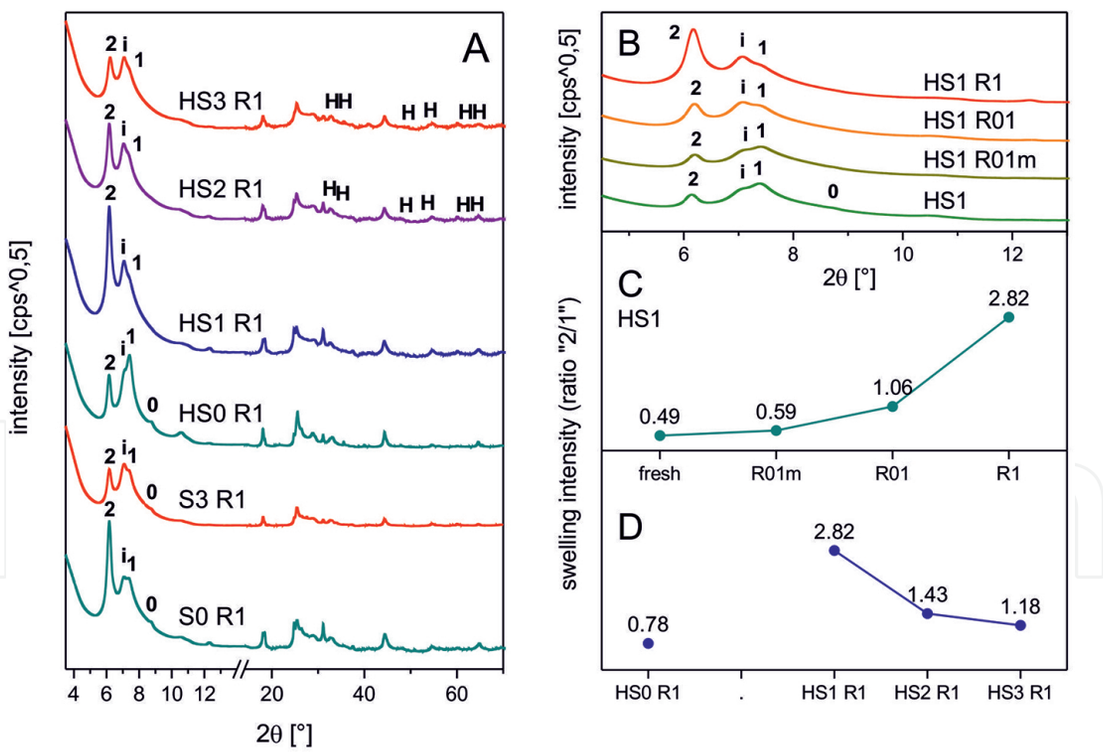

Figure 4. Structure of spent catalysts: A—vermiculite-supported iron oxide catalysts after reaction with phenol concentration 1 g/L; B and C—evolution of basal spacings of HS1 sample at different reaction conditions; D—evolution of basal spacings of nano-hematite-containing catalysts after reaction with phenol concentration 1 g/L; H—nano-hematite; 0, 1, 2—basal reflections of vermiculite corresponding to 0, 1, and 2 layers of interlayer water; i—interstratified vermiculite phases.

Sample name	*d* (nm)	*d* (nm)	*d* (nm)	*d* (nm)	*d* (nm)
Fresh catalysts (precipitated)					
S0	2.40	1.40	1.21	1.17	1.00
S2		1.43			1.01
S3		1.39			1.01
S4		1.37			1.01
Spent catalysts (precipitated)					
S0 H_2O_2	*	1.44	1.25	1.19	1.01
S0 R1	*	1.43	1.25	1.20	1.01
S3 R1	*	1.43	1.25	1.20	1.01
Fresh catalysts (hydrothermal)					
HS0	2.57	1.41	1.22	1.17	1.00
HS1	2.60	1.43	1.24	1.19	1.01
HS2	2.55	1.42	1.24	1.20	
HS3	2.53	1.39	1.22	1.18	
Spent catalysts (hydrothermal)					
HS0 R1	*	1.42	1.24	1.20	
HS1 R01m	*	1.42	1.24	1.19	
HS1 R01	*	1.43	1.25	1.20	
HS1 R1	*	1.43	1.25	1.20	
HS2 R01m	*	1.40	1.23	1.19	
HS2 R1	*	1.43	1.25	1.21	
HS3 R01	*	1.39	1.23	1.19	
HS3 R1	*	1.42	1.25	1.20	
	Interstratification	2 layers of water Mg^{2+}/Fe^{3+} in interlayers	Inter-stratification	1 layer of water Mg^{2+}/Fe^{3+} in interlayers	0 layers of water K^+ in interlayers

*2.4-2.6 nm (low-intensity peak).

Table 3. Interlayer distances of iron oxide-modified vermiculite-based catalysts before and after reaction.

The basal spacings calculated for modified vermiculites (**Table 3**) show that synthesis consisting on 2-line ferrihydrite precipitation resulted in the formation of hydroxy-interlayered phase and disappearance of peaks related to interstratified phases. Moreover, vermiculite was also partially intercalated with potassium. After the reaction, almost all peak positions returned to the initial values similar to the starting material. In nano-hematite modified samples, characteristic peaks for interstratification remained in their positions. However, in the course of phenol oxidation, first peak (~2.5 nm) became less noticeable.

It may be concluded that deposited iron oxide phases changed properties of the support; however, alteration was reversible in reaction conditions. Although XRD patterns do not allow to follow degradation of active phase directly, some indications of that process may be observed through properties of vermiculite.

More data considering properties of the deposited iron oxides were provided by DRS-UV-vis spectroscopy. As it was mentioned before, vermiculite itself contains iron [25] and UV-vis spectrum recorded for solid-state samples consisted of several characteristic bands. Isolated

Fe^{3+} cations in the tetrahedral coordination give rise to peaks at 224 nm in both silicate materials (S0 and HS0), and cations in the octahedral coordination may be identified by the presence of band at 260 nm [34, 35]. The bands at 319 and 358 nm are characteristic for small oligonuclear Fe_xO_y clusters. Formation of bulk Fe_2O_3 particles gave characteristic bands above 400 nm [34].

Ferrihydrite and hematite were characterized by multiple bands, revealed by the second derivative spectra (results not shown), and assigned to the electronic transitions [27, 36]. The spectra of both oxides consisted of peaks at 260–264 nm, which should be assigned to charge transfer. The bands at 401 and 424 nm for ferrihydrite and hematite, respectively, resulted from $^6A_1 \rightarrow {}^4E$; $^4A_1$ transition, 519 and 550 nm—$2(^6A_1) \rightarrow 2(^4T_1)$ (electron pair transition, EPT), 690–718 and 665 nm—$^6A_1 \rightarrow {}^4T_2$. Additionally, for nano-hematite, the following bands were assigned to $^6A_1 \rightarrow {}^4T_1$ transitions at 310 and 840 nm and $^6A_1 \rightarrow {}^4E$ transitions at 384 nm.

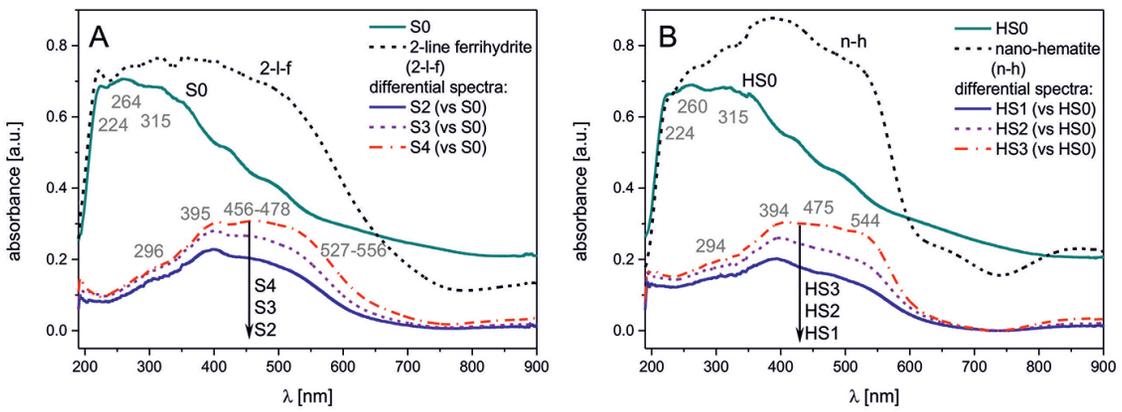

Figure 5. Agglomeration state of iron species in vermiculite-supported ferrihydrite- (A) and nano-hematite-containing (B) catalysts (DRS-UV-vis spectra).

Due to possible release of the cations from vermiculite and the contamination of deposited iron oxides during synthesis, the octahedra may be distorted, and consequently, ligand field and band positions may be changed. For 2-line ferrihydrite-containing catalysts, DRS-UV-vis peaks were shifted to 296, 456–478, 527–556, and 675 nm (**Figure 5A**). Similar result, with peak positions at 294, 442, 476, 544, 679, and 840 nm, was obtained for nano-hematite deposited on silicate (**Figure 5B**).

Further changes in the catalyst structure took place in the course of phenol oxidation. In the spectrum of starting silicate, S0, new band in the range of 360–480 nm was formed (**Figure 6A**). It is possible that adsorbed on the surface and interlayer Fe^{3+} cations present in original material were released and redeposited in the form of larger clusters. Catalysts modified with ferrihydrite after reaction with diluted phenol solution (R01) were depleted with active phase, and DRS-UV-vis spectra have shown minimum at 300 and 480 nm. Much larger minimum was registered in the differential spectrum of sample S3 after reaction with concentrated phenol solution. The shape and positions of minima (390, 453, and 524–550 nm) reflected distribution of absorption peaks in fresh catalyst. It may be expected that degradation of the catalyst is significant, although it is mechanical rather than chemical in nature.

http://dx.doi.org/10.5772/65097

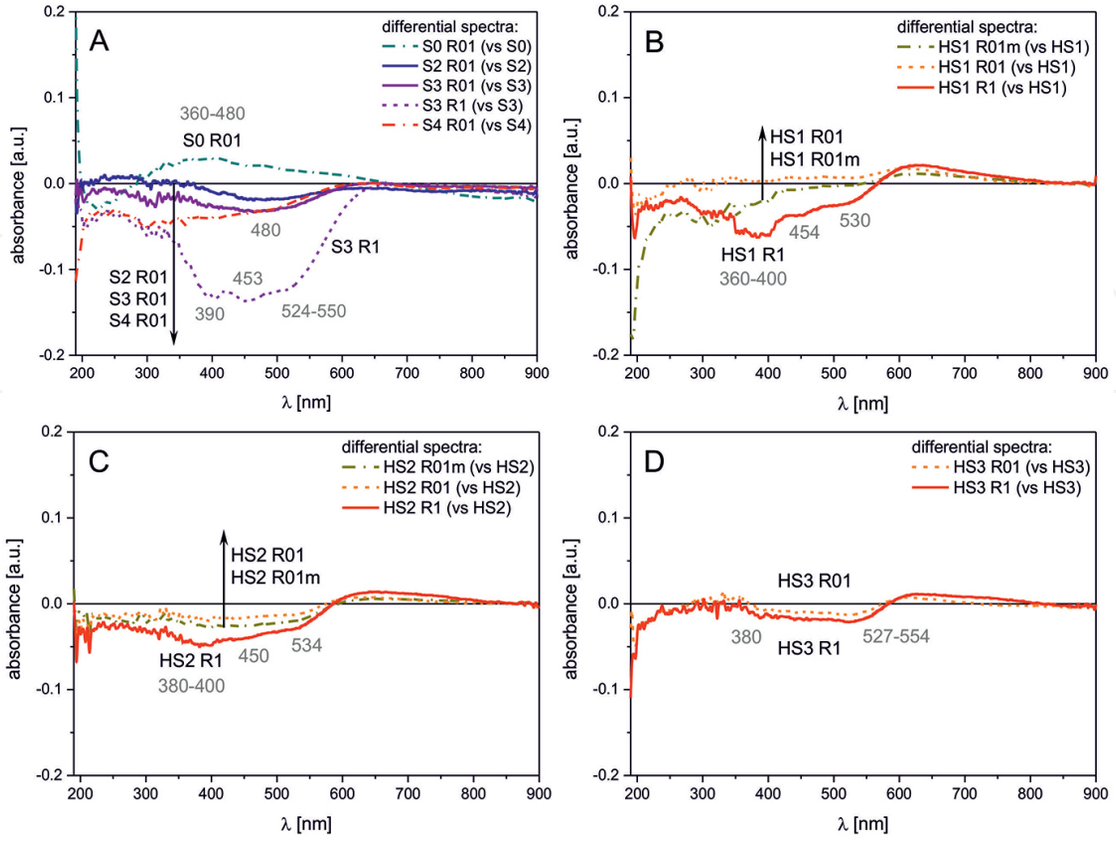

Figure 6. Leaching of iron species from vermiculite-supported iron oxide-containing catalysts upon phenol oxidation reaction (DRS-UV-vis spectra).

In nano-hematite-containing catalysts, degradation proceeded differently for each sample. At the lowest loading of active phase (**Figure 6B**, HS1), leaching was the most noticeable compared to the other samples, which were used in the reaction with concentrated substrates (R1). Moreover, the largest minimum was observed at 360–400 nm, while at 454 and 530 nm, two smaller features were observed. When the amount of hematite was increasing, minima recorded in DRS-UV-vis spectra were smaller and shifted to higher wavelengths (**Figure 6C/D**). Therefore, it may be concluded that optimization of the active phase loading is more important for hematite-containing composites, both in terms of catalyst stability and its activity. Surprisingly, although degradation of the catalysts is less noticeable in the reaction using lower concentration of phenol, the addition of lower excess of oxidant may also increase leaching of active components (e.g., **Figure 6B**). This feature may result in olation-oxolation processes, proceeding differently in the presence of H_2O_2.

On the basis of catalyst characterization, the following model was proposed for more active silicate-based nano-hematite-modified materials (**Figure 7**). In optimum conditions of about 3.36 wt.% of iron, which corresponds to 4.8 wt.% of deposited iron oxide, interlayer spaces of vermiculite are not blocked by hydroxides and are free to accommodate Fe^{3+} cations. On the surface of the layered support, patches of nanocrystalline phase are formed. Below the optimum hematite loading, besides well-defined nanocrystals, also oligomeric clusters of iron

oxide are deposited, which may be easily dissolved by the reaction substrates and products in the course of the reaction. The interlayer space of vermiculite is still available for an ion-exchange process. Above the optimum loading of the active phase, interlayer spaces of vermiculite are blocked by hydroxy-compounds, which may be removed during the reaction. Deposited nano-hematite phase remains almost intact during the reaction.

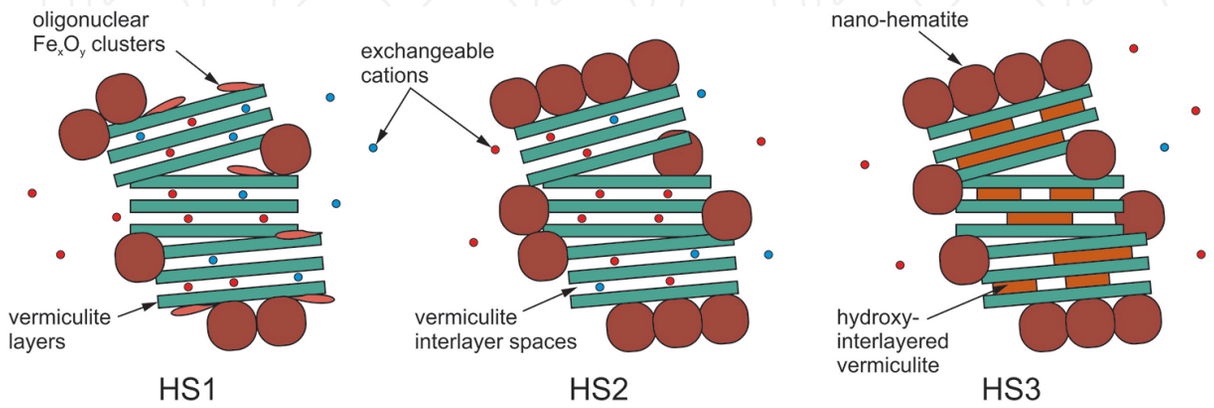

Figure 7. Simplified structure of nano-hematite-containing vermiculite-supported catalysts.

3.3. Catalytic activity vs. catalyst degradation

Changes in the catalyst chemical composition were followed during the reaction and correlated with catalytical results. In **Table 4**, it was presented that ferrihydrite-containing catalysts were more susceptible to Fe leaching. Surprisingly, the lower was oxide doping, the higher percentage of active phase was dissolved. No such straight relationship was observed for nano-hematite-containing catalysts. Apparently, small oligoclusters and interlayered hydroxy-species described in model in Section 3.2, indeed, contributed significantly to dissolved species. It was also observed that catalytic activity should not be attributed completely to homogeneous reaction. Reaction mixtures over ferrihydrite-doped catalysts were characterized with higher concentration of Fe available for homogeneous reaction. Times, required to obtain phenol conversion equal 40 and 50%, were longer for ferrihydrite-containing catalysts in comparison to hematite-doped materials. Moreover, in the latter case Fe concentrations in the reaction mixtures were relatively low. As it was described in Section 3.1, when diluted phenol solution was used for the reaction activity stagnated due to product accumulation. Another explanation could be recombination of radicals formed over the catalysts. Therefore, time for 50% phenol conversion is more or less 10 min delayed compared to 40% conversion. On the other hand, time difference for the reactions performed in concentrated phenol solution is closer to 1–3 min. Another conclusion may be formed on the basis of the analysis of residual phenol concentrations. Within 75 min of the reaction, phenol concentration is reduced to 3–31 and 2–6 mg/L for ferrihydrite- and hematite-containing catalysts, respectively, in reactions using starting solution equal to 100 mg/L. When 1 g/L phenol solution was used, final concentrations were equal to 8–11 and 15–30 mg/L for both iron containing series of catalysts. In this way, it

http://dx.doi.org/10.5772/65097

was confirmed that dispersed pollutants are more difficult to remove efficiently then concentrated.

Sample name	Fe content in catalyst (mg/g)	Fe available (mg/L)*	Fe leached from catalyst (%)**	PhOH residual (mg/L)*	$t_{40\%}$ (min)	$t_{50\%}$ (min)
S0	56.5					
S0 H_2O_2		1.0	1.0			
S0 R01		1.3	1.3	40	40	46
S0 R1		6.3	6.4	577	72	>75
S2	89.1					
S2 R01		5.7	3.6	26	32	44
S2 R1		n.d.	n.d.	11	52	54
S3	109.2					
S3 R01		4.6	2.4	31	34	46
S3 R1		27.1	14.0	21	29	32
S4	154.2					
S4 R01		2.8	1.0	3	40	50
S4 R1		n.d.	n.d.	8	28	29
HS0	59.0					
HS0 R01m		0.9	0.9	92	–	–
HS0 R01		0.5	0.4	35	32	49
HS0 R1		1.3	1.2	863	–	–
HS1	76.7					
HS1 R01m		3.2	2.3	89	–	62
HS1 R01		2.5	1.8	4	29	33
HS1 R1		26.0	19.2	19	41	43
HS2	86.8					
HS2 R01m		3.2	2.1	4	–	–
HS2 R01		1.0	0.7	2	24	26
HS2 R1		13.4	8.7	15	22	25
HS3	119.1					
HS3 R01		5.1	2.4	6	33	41
HS3 R1		23.9	11.4	30	30	33

n.d., not determined.
*In solution after 75 min of reaction.
**Percentage of initial content.

Table 4. Comparison of Fe content in catalysts and reaction solutions, residual concentration of phenol and time of 40 and 50% phenol conversion.

4. Conclusions

Depending on the experimental conditions, a nanocrystalline phase of hematite was formed in the hydrothermal synthesis. On the other hand, precipitation resulted in the formation of ferrihydrite phase. It was demonstrated that the latter phase is less active than nano-hematite; moreover, it was shown that optimum loading of the active phase is required to obtain the highest reaction efficiency: fast and high phenol conversion with minimum amount of side products as well as limited catalyst degradation. Among the transition products, formation of quinones was confirmed using derivative UV-vis spectroscopy. Physicochemical techniques also confirmed that nano-hematite-containing catalysts were more stable in studied reaction —only limited changes were observed in agglomeration state of Fe-containing materials, and leaching of iron was reduced. It was also shown that each group of catalysts is in different extents susceptible to degradation. However, the observed catalytic effect cannot be attributed only to homogeneous reaction. It was confirmed that dispersed pollutants are more resistant to degradation.

Author details

Agnieszka Węgrzyn

Address all correspondence to: a.m.wegrzyn@uj.edu.pl; a.m.wegrzyn@gmail.com

Faculty of Chemistry, Jagiellonian University in Krakow, Kraków, Poland

References

[1] Luck F. Wet air oxidation: past, present and future. Catalysis Today. 1999;53:81–91. DOI: 10.1016/S0920-5861(99)00112-1

[2] Busca G, Berardinelli S, Resini C, Arrighi L. Technologies for the removal of phenol from fluid streams: a short review of recent developments. Journal of Hazardous Materials. 2008;160:265–288. DOI:10.1016/j.jhazmat.2008.03.045

[3] Liotta LF, Gruttadauria M, Di Carlo G, Perrini G, Librando V. Heterogeneous catalytic degradation of phenolic substrates: catalysts activity. Journal of Hazardous Materials. 2009;162:588–606. DOI:10.1016/j.jhazmat.2008.05.115

[4] Rokhina EV, Virkutyte J. Environmental application of catalytic processes: heterogeneous liquid phase oxidation of phenol with hydrogen peroxide. Critical Reviews in Environmental Science and Technology. 2010;41:125–167. DOI:10.1080/10643380802669018

[5] Kim K-H, Ihm S-K. Heterogeneous catalytic wet air oxidation of refractory organic pollutants in industrial wastewaters: a review. Journal of Hazardous Materials. 2011;186:16–34. DOI:10.1016/j.jhazmat.2010.11.011

[6] He J, Yang X, Men B, Wang D. Interfacial mechanisms of heterogeneous Fenton reactions catalyzed by iron-based materials: a review. Journal of Environmental Sciences. 2011;39:97–109. DOI:10.1016/j.jes.2015.12.003

[7] Babuponnusami A, Muthukumar K. A review on Fenton and improvements to the Fenton process for wastewater treatment. Journal of Environmental Chemical Engineering. 2014;2:557–572. DOI:10.1016/j.jece.2013.10.011

[8] Wang N, Zheng T, Zhang G, Wang P. A review on Fenton-like processes for organic wastewater treatment. Journal of Environmental Chemical Engineering. 2016;4:762–787. DOI:10.1016/j.jece.2015.12.016

[9] Xu H-Y, Prasad M, Liu Y. Schorl: a novel catalyst in mineral-catalyzed Fenton-like system for dyeing wastewater discoloration. Journal of Hazardous Materials. 2009;165:1186–1192. DOI:10.1016/j.jhazmat.2008.10.108

[10] Matta R, Hanna K, Chiron S. Fenton-like oxidation of 2,4,6-trinitrotoluene using different iron minerals. Science of the Total Environment. 2007;385:242–251. DOI: 10.1016/j.scitotenv.2007.06.030

[11] Gomes Flores R, Layara Floriani Andersen S, Kenji Komay Maia L, Jorge José H, de Fatima Peralta Muniz Moreira R. Recovery of iron oxides from acid mine drainage and their application as adsorbent or catalyst. Journal of Environmental Management. 2012;111:53–60. DOI:10.1016/j.jenvman.2012.06.017

[12] Rahim Pouran S, Aziz Abdul Raman A, Mohd Ashri Wan Daud W. Review on the application of modified iron oxides as heterogeneous catalysts in Fenton reactions. Journal of Cleaner Production. 2014;64:24–35. DOI:10.1016/j.jclepro.2013.09.013

[13] Zelmanov G, Semiat R. Iron(3) oxide-based nanoparticles as catalysts in advanced organic aqueous oxidation. Water Research. 2008;42:492–498. DOI:10.1016/j.watres. 2007.07.045

[14] ElShafei GMS, Yehia FZ, Dimitry OIH, Badawi AM, Eshaq Gh. Ultrasonic assisted-Fenton-like degradation of nitrobenzene at neutral pH using nanosized oxides of Fe and Cu. Ultrasonics Sonochemistry. 2014;21:1358–1365. DOI:10.1016/j.ultsonch. 2013.12.019

[15] Pastrana-Martínez LM, Pereira N, Lima R, Faria JL, Gomes HT, Silva AMT. Degradation of diphenhydramine by photo-Fenton using magnetically recoverable iron oxide nanoparticles as catalyst. Chemical Engineering Journal. 2015;261:45–52. DOI:10.1016/ j.cej.2014.04.117

[16] Rusevova K, Kopinke F-D, Georgi A. Nano-sized magnetic iron oxides as catalysts for heterogeneous Fenton-like reactions—influence of Fe(II)/Fe(III) ratio on catalytic

performance. Journal of Hazardous Materials. 2012;241–242:433–440. DOI:10.1016/j.jhazmat.2012.09.068

[17] Chun J, Lee H, Lee S-H, Hong S-W, Lee J, Lee C, Lee J. Magnetite/mesocellular carbon foam as a magnetically recoverable fenton catalyst for removal of phenol and arsenic. Chemosphere. 2012;89:1230–1237. DOI:10.1016/j.chemosphere.2012.07.046

[18] Melero JA, Calleja G, Martínez F, Molina R, Pariente MI. Nanocomposite Fe_2O_3/SBA-15: an efficient and stable catalyst for the catalytic wet peroxidation of phenolic aqueous solutions. Chemical Engineering Journal. 2007;131:245–256. DOI:10.1016/j.cej.2006.12.007

[19] Shukla P, Wang S, Sun H, Ang H-M, Tadé M. Adsorption and heterogeneous advanced oxidation of phenolic contaminants using Fe loaded mesoporous SBA-15 and H_2O_2. Chemical Engineering Journal. 2010;164:255–260. DOI:10.1016/j.cej.2010.08.061

[20] Xiang L, Royer S, Zhang H, Tatibouët J-M, Barrault J, Valange S. Properties of iron-based mesoporous silica for the CWPO of phenol: a comparison between impregnation and co-condensation routes. Journal of Hazardous Materials. 2009;172:1175–1184. DOI:10.1016/j.jhazmat.2009.07.121

[21] di Luca C, Massa P, Fenoglio R, Medina Cabello F. Improved Fe_2O_3/Al_2O_3 as heterogeneous Fenton catalysts for the oxidation of phenol solutions in a continuous reactor. Journal of Chemical Technology and Biotechnology. 2014;89:1121–1128. DOI:10.1002/jctb.4412

[22] Aida Zubir N, Yacou C, Zhang X, Diniz da Costa JC. Optimisation of graphene oxide-iron oxide nanocomposite in heterogeneous Fenton-like oxidation of Acid Orange 7. Journal of Environmental Chemical Engineering. 2014;2:1881–1888. DOI:10.1016/j.jece.2014.08.001

[23] Shin S, Yoon H, Jang J. Polymer-encapsulated iron oxide nanoparticles as highly efficient Fenton catalysts. Catalysis Communications. 2008;10:178–182. DOI:10.1016/j.catcom.2008.08.027

[24] Yuan S-J, Dai X-H. Facile synthesis of sewage sludge-derived mesoporous material as an efficient and stable heterogeneous catalyst for photo-Fenton reaction. Applied Catalysis B: Environmental. 2014;154–155:252–258. DOI:10.1016/j.apcatb.2014.02.031

[25] Stawiński W, Freitas O, Chmielarz L, Węgrzyn A, Komędera K, Błachowski A, Figueiredo S. The influence of acid treatments over vermiculite based material as adsorbent for cationic textile dyestuffs. Chemosphere. 2016;153:115–129. DOI:10.1016/j.chemosphere.2016.03.004

[26] Węgrzyn A, Chmielarz L, Zjeżdżałka P, Jabłońska M, Kowalczyk A, Żelazny A, Vázquez Sulleiro M, Michalik M. Vermiculite-based catalysts for oxidation of organic pollutants in water and wastewater. Acta Geodynamica et Geomaterialia. 2013;10(171):341–352. DOI:10.13168/AGG.2013.0033

[27] Cornell RM, Schwertmann U. The Iron Oxides: Structures, Properties, Reactions, Occurrences and Uses. Weinheim: WILEY-VCH Verlag GmbH & Co. KGaA; 2003. DOI: 10.1002/3527602097

[28] Schwertmann U, Cornell RM. Iron Oxides in the Laboratory: Preparation and Characterization. Weinheim: WILEY-VCH Verlag GmbH & Co. KGaA; 2000. DOI: 10.1002/9783527613229

[29] Nakagawa H, Yamaguchi E. Influence of oxalic acid formed on the degradation of phenol by Fenton reagent. Chemosphere. 2012;88:183–187. DOI:10.1016/j.chemosphere.2012.02.082

[30] Harraz HZ, Hamdy MM. Interstratified vermiculite-mica in the gneiss-metapelite-serpentinite rocks at Hafafit area, Southern Eastern Desert, Egypt: from metasomatism to weathering. Journal of African Earth Sciences. 2010;58(2):305–320 DOI:10.1016/j.jafrearsci.2010.03.009

[31] Kalinowski BE, Schweda P. Rates and nonstoichiometry of vermiculite dissolution at 22°C. Geoderma. 2007;142(1–2):197–209. DOI:10.1016/j.geoderma.2007.08.011

[32] Mareschal L, Ranger J, Turpault MP. Stoichiometry of a dissolution reaction of a trioctahedral vermiculite at pH 2.7. Geochimica et Cosmochimica Acta. 2009;73(2):307–319. DOI:10.1016/j.gca.2008.09.036

[33] Abate G, Masini JC. Influence of thermal treatment applied to Fe(III) polyhydroxy cation intercalated vermiculite on the adsorption of atrazine. Journal of Agricultural and Food Chemistry. 2007;55:3555–3560. DOI:10.1021/jf063536y

[34] Kumar, MS, Schwidder, M, Grünert, W, Brückner, A. On the nature of different iron sites and their catalytic role in Fe-ZSM-5 DeNOx catalysts: new insights by a combined EPR and UV/VIS spectroscopic approach. Journal of Catalysis. 2004;227:384–397. DOI: 10.1016/j.jcat.2004.08.003

[35] Pérez-Ramirez, J, Santhosh Kumar, M, Brückner, A. Reduction of N_2O with CO over FeMFI zeolites: influence of the preparation method on the iron species and catalytic behavior. Journal of Catalysis. 2004;223:13–27, DOI:10.1007/s11144-014-0795-y

[36] Torrent J, Barrón V. Diffuse reflectance spectroscopy of iron oxides. In: Encyclopedia of Surface and Colloid Science, vol. 4, ed. Arthur T. Hubbard. Abingdon: Taylor & Francis; 2002. DOI:10.1081/E-ESCS

IntechOpen

IntechOpen